ARTICLE

BIOTECHNOLOGY and BIOENGINEERING

# A Strategy to Determine Operating Parameters in Tissue Engineering Hollow Fiber Bioreactors

R.J. Shipley,[1] A.J. Davidson,[2] K. Chan,[3] J.B. Chaudhuri,[2] S.L Waters,[1] M.J. Ellis[2]

[1]Oxford Centre for Industrial and Applied Mathematics, Mathematical Institute, 24–29 St. Giles', Oxford OX1 3LB, UK; telephone: 01865270744; fax: 01865270515; e-mail: shipley@maths.ox.ac.uk

[2]Centre for Regenerative Medicine, Department of Chemical Engineering, University of Bath, Bath, UK

[3]Centre for Mathematical Biology, Mathematical Institute, Oxford, UK

Received 12 September 2010; revision received 12 November 2010; accepted 7 December 2010

Published online 2 March 2011 in Wiley Online Library (wileyonlinelibrary.com). DOI 10.1002/bit.23062

**ABSTRACT:** The development of tissue engineering hollow fiber bioreactors (HFB) requires the optimal design of the geometry and operation parameters of the system. This article provides a strategy for specifying operating conditions for the system based on mathematical models of oxygen delivery to the cell population. Analytical and numerical solutions of these models are developed based on Michaelis–Menten kinetics. Depending on the minimum oxygen concentration required to culture a functional cell population, together with the oxygen uptake kinetics, the strategy dictates the model needed to describe mass transport so that the operating conditions can be defined. If $c_{\min} \gg K_m$ we capture oxygen uptake using zero-order kinetics and proceed analytically. This enables operating equations to be developed that allow the user to choose the medium flow rate, lumen length, and ECS depth to provide a prescribed value of $c_{\min}$. When $c_{\min} \not\gg K_m$, we use numerical techniques to solve full Michaelis–Menten kinetics and present operating data for the bioreactor. The strategy presented utilizes both analytical and numerical approaches and can be applied to any cell type with known oxygen transport properties and uptake kinetics.

Biotechnol. Bioeng. 2011;108: 1450–1461.



**KEYWORDS:** tissue engineering; bioreactor; oxygen; mass transport; mathematical modeling

## Introduction

Hollow fiber bioreactors (HFBs) are ideal for tissue engineering on a clinical scale because the large surface area to volume ratio will reduce the requirements of reagents, labor, and space: a hollow fiber system can be used to culture the same number of cells in 0.58 L as 1 $m^3$ using standard flask culture techniques (Ellis et al., 2005), and large cell numbers of up to $2 \times 10^8$ cell/mL can be obtained (Scragg, 1991). Knazek et al. (1972) were the first to report using a HFB for mammalian cell culture; since then the use of HFBs for mammalian cell expansion has become well documented (Tharakan and Chau, 1986) and several cell types have been cultured in HFBs including lymphocytes (Gramer and Poeschl, 2000; Gloeckner and Lemke, 2001), hepatocytes (Nyberg et al., 1994), and the osteogenic cell line 560pZIPv.neo (Ellis and Chaudhuri, 2007). There is extensive understanding of HFB fluid dynamics and mass transport obtained from experimental and modeling studies, and a wealth of data on tissue physiology and cell metabolism in vivo and in vitro. For example, Abdullah et al. (2009) and Abdullah and Das (2007) have focused on high-density bone cell populations, whereas hepatocyte culture has provided a focus for bioartificial liver development through studies such as Hay et al. (2000), Kawazoe et al. (2006), Nyberg et al. (2005), Patzer (2004), Sielaff et al. (1997), Sullivan et al. (2007), and Wurm et al. (2009). Together these studies provide insight into the interaction between the cell environment and the fluid dynamics and mass transfer of nutrients across the membrane. Oxygen is recognized as the limiting nutrient with respect to growth of a cell population and has been the most widely modeled (although glucose has also been considered). The uptake of oxygen is usually modeled using Michaelis–Menten kinetics, which captures the dependence on the uptake rate on the underlying concentration.

Correspondence to: R.J. Shipley

Contract grant sponsor: Christ Church, University of Oxford
Contract grant sponsor: Mathematical Institute, University of Oxford
Contract grant sponsor: Department of Chemical Engineering, University of Bath
Contract grant sponsor: John Fell Fund Oxford University Press Grant
Additional Supporting Information may be found in the online version of this article.

As a consequence of the nonlinear nature of Michaelis–Menten kinetics, numerical solutions to the transport equations associated with HFBs are commonly seen in literature. These use full Michaelis–Menten; examples of finite difference methods include Pillarella and Zydney (1990), whereas examples of finite element methods include Abdullah and Das (2007), Chen and Palmer (2010), Das (2007), Sullivan et al. (2007, 2008), and Ye et al. (2006). Analytical approaches have also been used in literature for situations where Michaelis–Menten can be approximated by zero- or first-order kinetics. Example of zero-order kinetics are Piret and Cooney (1991), whereas examples of first-order kinetics are Jayaraman (1992) and Kim and Cooney (1976). Although Kim and Cooney (1976) use first-order kinetics, the functional forms for the substrate concentrations that they determine are not dissimilar to those presented in this article. A good review of a range of transport models in HFBs is given by Brotherton and Chau (1996).

To ensure the efficacy of HFB for clinical applications it is necessary to have information that allows accurate and correct operation of the HFB. This article presents a tool to select the modeling approach best suited to obtain cell type-specific operating data. As such, the approach presented here differs significantly from existing studies in the literature. First of all, previous studies have considered only analytical or numerical solutions in isolation. Here we use both approaches, and specify how to differentiate between the two based on cell data. Secondly, the analytical solutions that we present are based on zero-order kinetics and have not been reported previously in the literature. Finally, a strategy is outlined for providing operating data (specifically the lumen length, extra-capillary space (ECS) depth, and lumen flow rate) that ensure the oxygen concentration throughout a HFB is held above a prescribed tissue-specific minimum. When an analytical approach is applicable this data takes the form of operating equations that relate the underlying parameters; for the numerical approach operating data are presented graphically. This strategy enables a user to fix the geometry (e.g., lumen length, ECS depth) and operating conditions (e.g., lumen length) of the bioreactor to obtain their required cell culture environment.

## Theory

### Setup

The fibers in a HFB fiber bundle are assumed to be Krogh cylinders, so that each fiber is identical and surrounded by an annulus of ECS containing a homogeneous distribution of cells (Krogh, 1918). The interstitial space between the Krogh cylinders is neglected as a modeling assumption. In this study, we consider transport in a single Krogh cylinder unit of a HFB bundle. This unit consists of a central lumen with a synthetic porous wall (referred to as the membrane), and surrounding ECS containing cells. Let $z$ be the axial direction down the lumen centerline, starting at the lumen inlet ($z=0$) with the lumen outlet denoted by $z=L$. We denote the radius of the lumen by $d$, the depth of the membrane by $s$ and the depth of the ECS by $l$. Typical values are $L=10$ cm, $d=100\,\mu$m, $s=20\,\mu$m, and $l=600\,\mu$m (Ye et al., 2007), although these should be varied as part of the bioreactor design process. A schematic of the setup is given in Figure 1.

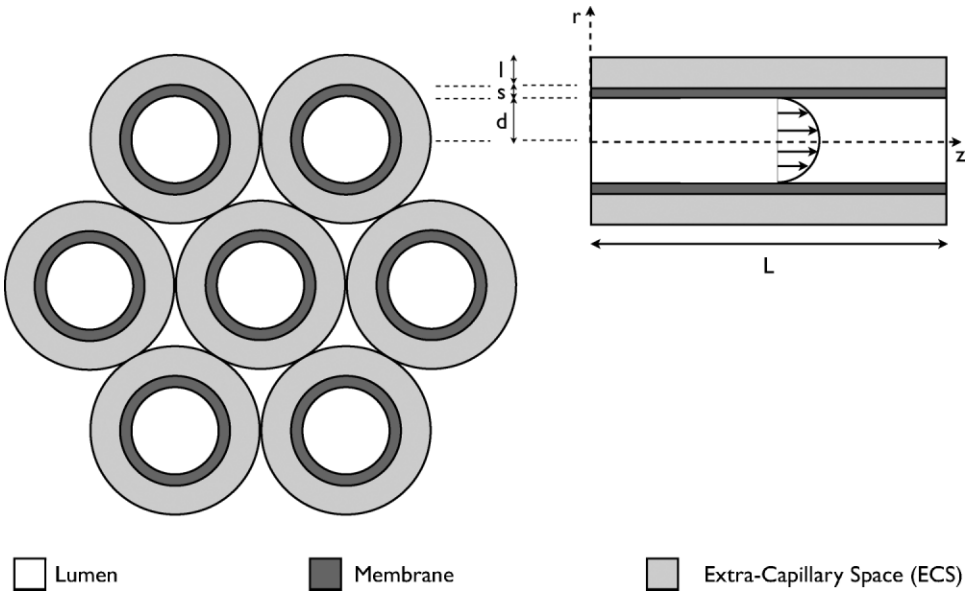


**Figure 1.** A schematic of the HFB setup. The left-hand schematic shows the structure of a fiber bundle, comprising seven Krogh cylinder units. The right-hand schematic shows a cross-section through an individual fiber, including the fluid velocity profile in the lumen.

Culture medium is pumped through the lumen at an imposed flowrate. There is no flow through the inlet to the membrane or ECS, so that fluid enters the system through the lumen only. Although this medium includes a mixture of solutes and proteins, we consider the transport of oxygen alone in this article. This is a widely adopted approach in the literature as oxygen is generally considered to be the rate-limiting nutrient, and reduces the complexity of the modeling process (Martin and Vermette, 2005; Piret and Cooney, 1991). Oxygen is transported by both advection (by the fluid) and diffusion in the lumen. Furthermore, oxygen diffuses through the membrane and ECS, where it is taken up by the cell population. In the analysis that follows we assume that the cell population is homogeneously distributed throughout the ECS, and neglect expansion of the cell population so that the parameters describing oxygen uptake are constant in time.

Fluid flow in the lumen is described by Poiseuille's law whereas flow in the membrane and ECS is neglected (this is a common modeling assumption for small aspect ratio HFB when there is not a significant pressure drop across the membrane or ECS (Brotherton and Chau, 1996; Piret and Cooney, 1991)). We denote this fluid velocity in the lumen by $\mathbf{u} = 2U(1-r^2/d^2)\mathbf{e}_z$, where $U$ is the mean velocity ($\mathrm{ms}^{-1}$), $r$ is the radial coordinate, and $\mathbf{e}_z$ is the unit vector in the $z$-direction. The oxygen concentration and flux are denoted by $c$ ($\mathrm{mol\,m}^{-3}$) and $\mathbf{J}$ ($\mathrm{mol\,m}^{-2}\,\mathrm{s}^{-1}$), respectively, with subscripts $l$, $m$, and $e$ denoting the values in the lumen, membrane, and ECS, respectively. The oxygen fluxes are

$$\mathbf{J}_l = c_l\mathbf{u} - D_l\nabla c_l, \quad \mathbf{J}_m = -D_m\nabla c_m, \quad \mathbf{J}_e = -D_e\nabla c_e, \quad (1)$$

where $D_l$, $D_m$, and $D_e$ are the diffusion coefficients for oxygen in the lumen, wall, and ECS, respectively (all assumed constant, with units $\mathrm{m}^2\,\mathrm{s}^{-1}$). The lumen oxygen flux is comprised of advection due to the fluid velocity, together with diffusion; the membrane and ECS fluxes are comprised of diffusion only. The conservation equations for the concentration of oxygen in each of the regions are:

$$\begin{aligned} &\frac{\partial c_l}{\partial t} + \nabla\cdot\mathbf{J}_l = 0 \text{ in the lumen,}\\ &\frac{\partial c_m}{\partial t} + \nabla\cdot\mathbf{J}_m \text{ in the membrane,}\\ &\frac{\partial c_e}{\partial t} + \nabla\cdot\mathbf{J}_e + R(c_e) = 0 \text{ in the ECS,} \end{aligned} \quad (2)$$

where the reaction term $R(c_e)$ captures the uptake of oxygen by the cells. We will assume Michaelis–Menten kinetics for this reaction term, so that

$$R(c_e) = \frac{V_{\max}c_e}{c_e + K_m}. \quad (3)$$

It is necessary to prescribe boundary conditions on the internal and external boundaries of the bioreactor. On the lumen/membrane and membrane/ECS boundaries we prescribe continuity of concentration and flux, so that

$$c_l = c_m \quad \text{and} \quad \mathbf{J}_l\cdot\mathbf{n} = \mathbf{J}_m\cdot\mathbf{n} \quad \text{on the lumen/membrane boundary,} \quad (4)$$

$$c_m = c_e \quad \text{and} \quad \mathbf{J}_m\cdot\mathbf{n} = \mathbf{J}_e\cdot\mathbf{n} \quad \text{on the membrane/ECS boundary,} \quad (5)$$

where $\mathbf{n}$ is the unit outward pointing normal to the relevant surface. Finally we prescribe the oxygen concentration as $c_{\mathrm{in}}$ ($\mathrm{mol\,m}^{-3}$) at the lumen inlet (where $c_{\mathrm{in}}$ may be chosen to suit the application under consideration), and impose no flux of concentration out of the outer ECS boundary,

$$c_l = c_{\mathrm{in}} \quad \text{on } z = 0, \quad \text{and} \quad \mathbf{J}_e\cdot\mathbf{n} = 0 \quad \text{on the outer ECS boundary.} \quad (6)$$

The assumption of no flux out of the outer boundary is analogous to a symmetry condition representation of a bundle of fibers. It compares directly to the Krogh cylinder approach used frequently in the literature.

Next the solution of the model (2)–(6) is considered using numerical or analytical techniques. For both strategies a steady-state solution is sought and it is assumed that a 2D axisymmetric geometry is described by the radial coordinate $r = \sqrt{x^2 + y^2}$ and the axial coordinate $z$.

## Analytical Approach

To pursue an analytical approach, the system of equations given by (2)–(6) can be simplified with various assumptions. First of all the small aspect ratio of a fiber is exploited, defined by $\varepsilon = d/L \approx 1\times10^{-3} \ll 1$. It should be noted that whilst the lumen radius, $d$ and fiber length, $L$ can both be varied as part of the design process so that neither $d$ nor $L$ are fixed, $\varepsilon \ll 1$ will be maintained throughout.

It is not possible to make progress analytically using the nonlinear Michaelis–Menten reaction term given by (3). Therefore, we assume that $c_e \gg K_m$ so that the reaction term $R(c_e)$ can be approximated by $V_{\max}$. This is an important assumption and means that predictions of the analytical model are only valid when the ECS oxygen concentration is much larger than the half-maximal oxygen concentration. As such, for cell types where the demand for oxygen is similar to, or smaller than, $K_m$ it will not be appropriate to use the analytical model (in this scenario a numerical approach should be used, as outlined later in the article).

Finally the relative importance of advection and diffusion in the lumen is evaluated by considering the Péclet number, $Pe = UL/D_l$. In fact it is the reduced Péclet number, $Pe^* = \varepsilon^2 Pe = Ud^2/LD_l$, that is critical for this system, as it also takes account of the small aspect ratio of the lumen (it is analogous to the *reduced Reynolds number* that was used to

characterize fluid transport for a similar study in Shipley et al. (2010)). A large reduced Péclet number indicates an advection-dominated regime, whereas a small reduced Péclet number indicate a diffusion-dominated regime. Typically for this system $U \approx 1\,\mathrm{cm\,s^{-1}}$, $L \approx 10\,\mathrm{cm}$, and $D \approx 10^{-9}\,\mathrm{m^2\,s^{-1}}$, giving $Pe^* \approx 1$ so that advection and diffusion are both important in the lumen. It is assumed that $Pe^* = \varepsilon^2 Pe$ is of order 1 in the analysis that follows. For the mathematical detail of the reduction of (2)–(6) based on the assumptions above, together with the solution of the resulting model, please refer to the Supplementary Material A.

The outer radius of the lumen, membrane and ECS (each measured from the lumen centerline) are denoted by $R_l$, $R_w$, and $R_e$ so that $R_l = d$, $R_m = d + s$, and $R_e = d + s + l$. The following dimensionless parameters are also defined:

$$Pe^* = \frac{Ud^2}{LD_l}, \quad M = \frac{d^2 V_{\max}}{D_e c_{\mathrm{in}}}, \tag{7}$$

which capture the key physical features of the system. As described above, $Pe^*$ is the reduced Péclet number and is assumed to be of order 1. The parameter $M$ represents the balance of oxygen consumption versus diffusion in the ECS, and can take a range of values depending on the relative importance of these effects.

The analysis described above and in the Supplementary Material results in the following expressions for the oxygen concentration throughout the module:

$$\frac{c_l}{c_{\mathrm{in}}} = 1 + \frac{\gamma r}{d} + \sum_{n=0}^{\infty} E_n \exp\left(\frac{\lambda_n r^2}{2d^2}\right) \mathrm{KummerM}\left(\frac{1}{2} + \frac{\lambda_n}{4}, 1, -\frac{\lambda_n r^2}{d^2}\right) \times \left[G_n \exp\left(-\frac{\lambda_n^2 z}{2Pe^* L}\right) + \frac{F_n}{\lambda_n^2}\right], \tag{8}$$

$$\frac{c_m}{c_{\mathrm{in}}} = \frac{MD_e}{2D_m d^2}(R_m^2 - R_e^2)\ln\frac{r}{d} + B(z), \tag{9}$$

$$\frac{c_e}{c_{\mathrm{in}}} = \frac{M}{4d^2}\left[r^2 - R_m^2 + \frac{2D_e}{D_m}(R_m^2 - R_e^2)\ln\left(\frac{R_m}{d}\right) + 2R_e^2 \ln\left(\frac{R_m}{r}\right)\right] + B(z), \tag{10}$$

where

$$B(z) = 1 + \gamma + \sum_{n=0}^{\infty} E_n \exp\left(\frac{\lambda_n}{2}\right) \mathrm{KummerM}\left(\frac{1}{2} + \frac{\lambda_n}{4}, 1, -\lambda_n\right) \times \left[G_n \exp\left(-\frac{\lambda_n^2 z}{2Pe^* L}\right) + \frac{F_n}{\lambda_n^2}\right], \tag{11}$$

and

$$\gamma = \frac{MD_e}{2D_l d^2}[R_m^2 - R_e^2]. \tag{12}$$

Here "KummerM $(\mu, \nu, x)$" is the confluent hypergeometric function and is a solution of a specific differential equation, as described in the Supplementary Material A (and discussed in Abramowitz and Stegun, 1965). Further $\lambda_n$, $E_n$, $F_n$, and $G_n$ for $n = 0, \ldots, \infty$ are constants. The $\lambda_n$ and $E_n$ are the eigenvalues and normalization constants for the Sturm–Liouville problem associated with the system (2)–(4); these are constants independent of the geometry or cell population properties and are provided in the Supplementary Material B for $n = 0, \ldots, 49$. By contrast $F_n$ and $G_n$ are coefficients in a Sturm–Liouville expansion of two different functions, and depend explicitly on the cell population properties (specifically the consumption rate of oxygen) and the geometry of the bioreactor (specifically the radius of the lumen and depths of the membrane and ECS).

Although Equations (8)–(10) appear complex, the behavior that they describe is relatively straightforward to understand: the oxygen concentration in the lumen, membrane, and ECS depends on the radial distance from the lumen centerline. Each solution is also dependent on the distance down the lumen centerline, $z$, as a consequence of advection in the lumen. This is transmitted into the membrane and ECS regions through the function $B(z)$, which is the lumen concentration value on the lumen wall (i.e., the solution in (8) when $r = R_l = d$). This function $B(z)$ reveals that the concentration decays exponentially down the lumen from a maximum value at the inlet $z = 0$. The remaining terms in the solution for $c_m$ and $c_e$ in (9) and (10) describe the radial decay of the oxygen concentration from the outer surface of the membrane as a consequence of oxygen uptake by the cells in the ECS.

Through cell-specific design criteria, we must design the bioreactor to ensure that the oxygen concentration exceeds a prescribed minimum throughout the bioreactor. This minimum oxygen concentration will be achieved at the furthest distance from the inlet, that is, when $r = R_e$ and $z = L$. Denoting this minimum value by $c_{\min}$, the analytical method gives the following expression for $c_{\min}$, in terms of experimentally controlled and cell-specific parameters:

$$\frac{c_{\min}}{c_{\mathrm{in}}} = \frac{M}{4d^2}\left[R_e^2 - R_m^2 + \frac{2D_e}{D_m}(R_m^2 - R_e^2)\ln\left(\frac{R_m}{d}\right) + 2R_e^2 \ln\left(\frac{R_m}{R_e}\right)\right] + B(L). \tag{13}$$

## Numerical Approach

For the analytical approach, the full system given by (2)–(6) is solved using finite element method package "COMSOL

Multiphysics 3.5a"[1] to evaluate the dependence of the oxygen concentration on the underlying parameters. The numerical approach is valid for all concentration values; however, the full system of equations must be solved iteratively each time. This is a computationally intensive process and does not provide operating equations that describe the dependence of the minimum oxygen concentration on the underlying parameters. Therefore, the numerical approach will be used when the analytical approach is not valid, that is, when $c_{\min} \not\gg K_m$. The mesh used for the results in this article consists of approximately 7,000 finite elements (and refining the mesh to 29,312 elements did not change the results to three significant figures).

## Results and Discussion

The analytical and numerical methodologies outlined in the Theory Section will be used to outline a strategy for developing cell-specific operating criteria for the bioreactor. These criteria will then be tested for specific cell types.

### Strategy for Developing Optimal Operating Conditions

To develop operating conditions, it is necessary to understand how the minimum oxygen concentration depends on the geometrical properties of the bioreactor, together with the parameters that can be controlled experimentally. Through this understanding, the HFB can be designed to optimally grow cells of a particular type.

Once a cell type and seeding density are chosen the following parameters are fixed:

(1) The maximal oxygen consumption rate, $V_{\max}$.
(2) The half-maximal oxygen concentration, $K_m$.
(3) The diffusivity of oxygen in the ECS, $D_e$.

The diffusivity of oxygen in the lumen and membrane ($D_l$ and $D_m$, respectively) are known from the literature or experiments. The outer radii of the lumen and membrane ($R_l$ and $R_m$, respectively) are fixed, and there are specific values of the lumen inlet concentration $c_{\text{in}}$ and minimum oxygen concentration $c_{\min}$ that must be achieved. So, the bioreactor design parameters that are left to be determined are:

(1) The depth of the ECS, $l$ (which determines $R_e$).
(2) The length of the lumen, $L$.

[1]Developed and distributed by COMSOL, Inc. Full details available online at http://www.comsol.com/.

Finally, the mean inlet flow rate $U$ can be controlled by fixing the volumetric flow rate on the pump used to deliver fluid to the bioreactor.

If $c_{\min} \gg K_m$ the analytical approach is valid and the results from the Analytical Approach Section can be used to fix $l$, $L$, and $U$; however, if $c_{\min} \gg K_m$ the analytical approach is not valid, and the numerical method must instead be used. These two approaches are detailed below.

**$c_{\min} \gg K_m$** The operating conditions are specified for the bioreactor using Equation (13) for the minimum oxygen concentration. When the parameters described above are fixed, only $R_e$ and the ratio $U/L$ (through $Pe^*$) can be determined independently using the analytical approach. Two cases will be considered:

(1) The outer radius of the ECS, $R_e$ is fixed, and so $Pe^*$ can be determined.
(2) The ratio $U/L$ (and therefore $Pe^*$) is fixed, and so $R_e$ can be determined.

For the first case it is assumed that the outer radius of the ECS is fixed so that $R_e$ (and thus $\gamma$, $F_n$, and $G_n$ for $n = 0, \ldots, \infty$) is known. In this case, (13) can be written as the following operating equation for $c_{\min}$ in terms of the reduced Péclet number $Pe^*$:

$$\frac{c_{\min}}{c_{\text{in}}} = A + \sum_{n=0}^{\infty} B_n \exp\left(-\frac{\lambda_n^2}{2Pe^*}\right) + C_n, \tag{14}$$

where

$$A = \frac{M}{4d^2}\left[R_e^2 - R_m^2 + \frac{2D_e}{D_m}(R_m^2 - R_e^2)\ln\left(\frac{R_m}{d}\right) + 2R_e^2\ln\left(\frac{R_m}{R_e}\right)\right] + 1 + \gamma, \tag{15}$$

$$B_n = E_n G_n \exp\left(\frac{\lambda_n}{2}\right)\text{KummerM}\left(\frac{1}{2} + \frac{\lambda_n}{4}, 1, -\lambda_n\right),$$
$$C_n = \frac{E_n F_n}{\lambda_n^2}\exp\left(\frac{\lambda_n}{2}\right)\text{KummerM}\left(\frac{1}{2} + \frac{\lambda_n}{4}, 1, -\lambda_n\right), \tag{16}$$

are all fixed constants. Given the values of these constants, (14) can be used to determine the value of $Pe^*$ (and hence the ratio $U/L$) that provides the required value of $c_{\min}$ (note that it is this ratio rather that the individual values of $U$ and $L$ that influence the minimum oxygen concentration). Equation (14) shows that the minimum oxygen value $c_{\min}$ decreases exponentially as the lumen length $L$ increases, or the lumen velocity $U$ decreases. This means that for a lower $c_{\min}$ requirement, a smaller flow velocity and longer fiber can be used.

Next it is assumed that the ratio $U/L$ is prescribed so that $Pe^*$ is given. Now the operating equation for $c_{\min}$ in terms of the ECS depth is:

$$\frac{c_{\min}}{c_{\text{in}}} = K + QR_e^2 - \frac{2M}{d^2}R_e^2\ln(R_e/d) + \sum_{n=0}^{\infty}(H_nG_n + J_nF_n), \tag{17}$$

where

$$K = \frac{M}{4d^2}\left[\frac{2D_eR_m^2}{D_m}\ln\left(\frac{R_m}{d}\right) - R_m^2\right] + 1 + \frac{MD_eR_m^2}{2D_ld^2},$$
$$Q = \frac{M}{4d^2}\left(1 + 2\ln\left(\frac{R_m}{d}\right)\left(1 - \frac{D_e}{D_m}\right) - \frac{2D_e}{D_l}\right), \tag{18}$$

$$H_n = E_n\exp\left(\frac{\lambda_n}{2}\right)\text{KummerM}\left(\frac{1}{2} + \frac{\lambda_n}{4}, 1, -\lambda_n\right)\exp\left(-\frac{\lambda_n^2}{2Pe^*}\right),$$
$$J_n = \frac{E_n}{\lambda_n^2}\exp\left(\frac{\lambda_n}{2}\right)\text{KummerM}\left(\frac{1}{2} + \frac{\lambda_n}{4}, 1, -\lambda_n\right), \tag{19}$$

are all fixed constants. Given the values of these constants, (17) depends on $R_e$ through the explicit appearance of $R_e$ in (17) as well as $G_n$ and $F_n$ for $n = 0, \ldots, \infty$. For a given value of $c_{\min}$, (17) can therefore be solved numerically to determine $R_e$.

**$c_{\min} \not\gg K_m$**: In this scenario the numerical approach will be used, as outlined in Numerical Approach Section.

## Cell Types and Parameter Values

The parameters that will be kept fixed in our investigation are:

(1) The oxygen diffusivities $D_l = 3\times10^{-9}\,\text{m}^2\,\text{s}^{-1}$, $D_m = 3\times10^{-10}\,\text{m}^2\,\text{s}^{-1}$, and $D_e = 6\times10^{-9}\,\text{m}^2\,\text{s}^{-1}$ (Ye et al., 2006).
(2) The lumen radius $R_l = d = 100\,\mu\text{m}$ and the depth of the membrane $s = 20\,\mu\text{m}$ (so that $R_m = 120\,\mu\text{m}$) (Ye et al., 2006).
(3) The inlet oxygen concentration will be fixed for each individual cell type.

The kinetic data (i.e., $V_{\max}$ and $K_m$) for a range of cell types, sourced from combined modeling and experimental studies in the literature, are shown in Table I. For cardiomyocytes, hepatocytes, and pancreatic cells we fix $c_{\text{in}} = 0.22\,\text{mol}\,\text{m}^{-3}$ (as is standard for culture medium Piret and Cooney, 1991). However, chondrogenic differentiation is limited when the oxygen concentration exceeds approximately $0.1\,\text{mol}\,\text{m}^{-3}$ (Lund-Olesen, 1970; Treuhaft and McCarty, 1971); therefore $c_{\text{in}} = 0.1\,\text{mol}\,\text{m}^{-3}$ is used for chondrocytes.

## Validation of Analytical and Numerical Approaches

The analytical approach is a reduction of the full model given by (2)–(6) and therefore should be validated. This validation could be performed against experimental data; however, this data is difficult to collect accurately and is not

**Table I.** Oxygen uptake and culturing data for a range of cell types.

| Cell type | $V_{\max}$ ($\text{mol}\,\text{m}^{-3}\,\text{s}^{-1}$) | $K_m$ ($\text{mol}\,\text{m}^{-3}$) | Cell density ($\text{cells}\,\text{m}^{-3}$) | $c_{\min}$ ($\text{mol}\,\text{m}^{-3}$) | $c_{\text{in}}$ ($\text{mol}\,\text{m}^{-3}$) | Source |
|---|---|---|---|---|---|---|
| Neonatal rat cardiomyocytes | $2.64\times10^{-3}$ | $6.9\times10^{-3}$ | $10^{12}$ | $8\times10^{-2}$ | 0.22 | Radisic et al. (2005) |
| | | | | $6\times10^{-3}$ | | Carrier et al. (1999) |
| Primary rat hepatocytes | $1.76\times10^{-3}$ | $6.24\times10^{-3}$ | $1.25\times10^{13}$ | $2.1\times10^{-2}$ | 0.22 | Sullivan et al. (2007) |
| | | | | | | Consolo et al. (2008) |
| Pancreatic βTC3 cells | $6.37\times10^{-3}$ | $1.0\times10^{-2}$ | $2.8\times10^{14}$ | $1.46\times10^{-2}$ | 0.22 | Tziampazis and Sambanis (1995) |
| | | | | | | Stabler et al. (2009) |
| Bovine chondrocytes | $4.8\times10^{-5}$ | $5.0\times10^{-3}$ | $1.4\times10^{14}$ | $1\times10^{-2}$ | 0.1 | Malda et al. (2004) |
| | | | | $1.32\times10^{-2}$ | | Obradovic et al. (1999, 2000) |
| | | | | $2.2\times10^{-3}$ | | Fermor et al. (2007) |

For a description of the various minimum oxygen concentrations, please refer to the main text. The $V_{\max}$ value for neonatal rat cardiomyocytes and primary rat hepatocytes have been multiplied by a cell volume fraction of 0.3, as per the modeling in Sullivan et al. (2007). For the pancreatic cells it has also been assumed that each cell has a 10 μm diameter.

Note: For neonatal rat cardiomyocytes two values are listed. It has been observed that cardiac constructs cultivated in perfusion at oxygen concentrations of ~80 μM exhibit weaker presence of cardiac markers and poorer organization of contractile apparatus compared with constructs cultivated at oxygen concentrations of ~200 μM Carrier et al. (1999); this explains the first value. The second value (6 μM) is a typical hypoxia value (Radisic et al., 2005). The $c_{\min}$ value for primary rat hepatocytes is based the critical threshold value of 10 mmHg quoted in the literature Consolo et al. (2008) (and transferred from a partial pressure into a concentration using Henry's law with an oxygen solubility value of 2.08 $\text{mmol}\,\text{m}^{-3}\,\text{mmHg}$). For pancreatic βTC3 cells, published experiments found that oxygen tensions above 7 mmHg were required for the cells to retain their secretory capacity Stabler et al. (2009); using Henry's law gives the value in Table I. Finally, a range of minimum oxygen concentrations are presented for articular cartilage in the literature. In Obradovic et al. (1999), it is hypothesized that articular cartilage is exposed to a minimum oxygen concentration in the range 0.01 $\text{mol}\,\text{m}^{-3}$ to 0.08 $\text{mol}\,\text{m}^{-3}$ in vivo, where lower oxygen concentrations are not detrimental to chondrocyte viability but can impact synthesis of extracellular matrix; this explains the first $c_{\min}$ value in Table I. In Fermor et al. (2007), it is reported that the superficial zone of articular cartilage exists at above approximately 6% oxygen concentration, whereas the deep zone exists at <1%; this explains the final two $c_{\min}$ values of Table I.

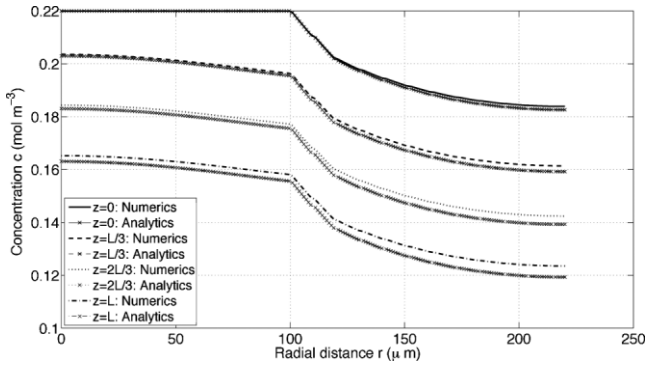


**Figure 2.** Comparison of the analytical and numerical approaches. The graph shows the radial oxygen concentration profiles for primary rat hepatocytes (see Table I) at fixed values of $z$, using both the analytical and numerical techniques. The fixed parameters are $U = 1 \times 10^{-2}$ ms$^{-1}$, $L = 10$ cm, and $R_e = 220$ μm.

presented in sufficient detail in the literature. Given that the numerical approach is valid for all concentration values and solves the full model (2)–(6), it is appropriate to validate results of the analytical model against numerical solutions. This comparison is shown in Figure 2, where radial oxygen concentration profiles are shown (at fixed values $z = 0$, $L/3$, $2L/3$, $L$) for the primary rat hepatocyte data in Table I (Sullivan et al., 2007) when $U = 1 \times 10^{-2}$ m/s, $L = 10$ cm, $R_e = 220$ μm. For the analytical solutions, all sums have been truncated at 50 terms, that is, $n = 49$, for ease of computation. The agreement between the analytical and numerical results is very strong, although it becomes weaker as the concentrations decrease. The lowest concentration value is at the ECS outlet (when $r = R_e$ and $z = L$); here both the analytical and numerical concentration values are 0.12 mol m$^{-3}$ to two decimal places, with a percentage difference of 3.39% (which is within experimental error).

## Analytical and Numerical Results

It must first be decided whether to use the analytical or numerical strategy to provide operating data. Table II provides a summary of this decision making process. Data on $c_{\min}$ and $K_m$ are provided for each cell type, together with the value of the ratio $c_{\min}/K_m$. The analytical model is valid when $c_{\min} \gg K_m$; here we choose a value of the ratio $c_{\min}/K_m = 2$ as the critical value so that if $c_{\min}/K_m > 2$ the analytical model is used, whereas if $c_{\min}/K_m > 2$ the numerical approach is used. Different critical values of $c_{\min}/K_m$ could certainly be implemented, even on a cell-specific basis. The errors associated with using $c_{\min}/K_m = 2$ as the critical value are within the bounds of experimental error, and the errors associated with other modeling assumptions (e.g., the Krogh cylinder approximation). On this basis, the analytical model is appropriate for the cardiomyocytes ($c_{\min} = 8 \times 10^{-2}$ mol m$^{-3}$), hepatocytes, and chondrocytes ($c_{\min} = 1.32 \times 10^{-2}$ mol m$^{-3}$), whereas the numerical model is used for the remaining examples in Table II. We present

**Table II.** Use of the analytical or numerical models. If $c_{\min}/K_m > 2$, the analytical model is used; otherwise the numerical model is used.

| Cell type | $c_{\min}/c_{\text{in}}$ | $K_m/c_{\text{in}}$ | $c_{\min}/K_m$ | Analytical model | Numerical model |
|---|---|---|---|---|---|
| Neonatal rat cardiomyocytes | 0.36 | 0.031 | 11.6 | ✓ | × |
| | 0.027 | 0.031 | 0.87 | × | ✓ |
| Primary rat hepatocytes | 0.095 | 0.028 | 3.4 | ✓ | × |
| Pancreatic βTC3 cells | 0.066 | 0.045 | 1.5 | × | ✓ |
| Bovine chondrocytes | 0.1 | 0.05 | 2.0 | × | ✓ |
| | 0.13 | 0.05 | 2.64 | ✓ | × |
| | $2.2 \times 10^{-2}$ | 0.05 | 0.44 | × | ✓ |

data for the extreme cases of high and low oxygen requirements, that is, cardiomyocytes and chondrocytes, respectively.

Figures 3a–c and 5a–c show the variation in $c_{\min}/c_{\text{in}}$ (with $c_{\text{in}}$ fixed) as a function of $1/Pe^*$ for fixed $R_e$, as described by operating equation (14), for the cardiomyocytes and chondrocytes, respectively. As would be anticipated, $c_{\min}$ is largest for low values of $1/Pe^*$, corresponding to either a large lumen velocity $U$ or shorter lumen length $L$ (a larger $U$ ensures increased delivery of oxygen to the cells through advection, whereas a shorter lumen length decreases the distance of the furthermost cells from the oxygen source). For each value of $R_e$ the maximum variation in $c_{\min}/c_{\text{in}}$ is of size $10^{-2}$, indicating that $c_{\min}$ is only weakly sensitive to the value of $Pe^*$. For $Pe^* < 2$ (i.e., $1/Pe^* > 0.5$) $c_{\min}$ is virtually constant, indicating a linear relationship between the values of $U$ and $L$ required to achieve a chosen value of $c_{\min}$.

Given that this linear relationship is representative of the low $c_{\min}$ regime, it is mimicked by the numerical results of Figures 4 and 6. These figures show how the critical lumen length, $L_{\text{crit}}$ say, required to satisfy the minimum oxygen concentrations of Table I varies as a function of the lumen velocity $U$. For each cell type four different values of $R_e$ were tested, each of which demonstrates a linear relationship between $L_{\text{crit}}$ and $U$ (with correlation factor 0.99). These figures can be used to read off a required $L_{\text{crit}}$ and $U$ value to satisfy the minimum oxygen requirements summarized in Table I. For example, for the cardiomyocytes with $R_e = 270$ μm with a lumen length of 10 cm, a lumen flow velocity of $U \approx 9 \times 10^{-3}$ m s$^{-1}$ will ensure $c > 6 \times 10^{-3}$ mol m$^{-3}$ throughout the module.

In contrast, Figures 3d and 5d show the variation in $c_{\min}/c_{\text{in}}$ (with $c_{\text{in}}$ fixed in each case) as a function of $R_e$ for fixed $Pe^*$, as described by operating equation (17), for the cardiomyocytes and chondrocytes, respectively. As anticipated, $c_{\min}$ decreases as the ECS depth (i.e., $R_e$) increases. The rate of this decay is heavily dependent on the uptake rate of oxygen by the cell population, $V_{\max}$, which is largest for the cardiomyocytes, and lowest for the chondrocytes. For example, a value of $c_{\min}/c_{\text{in}} = 0.2$ is sustained by the cardiomyocytes, hepatocytes, and chondrocytes when $R_e \approx 267$ and 720 μm, respectively.

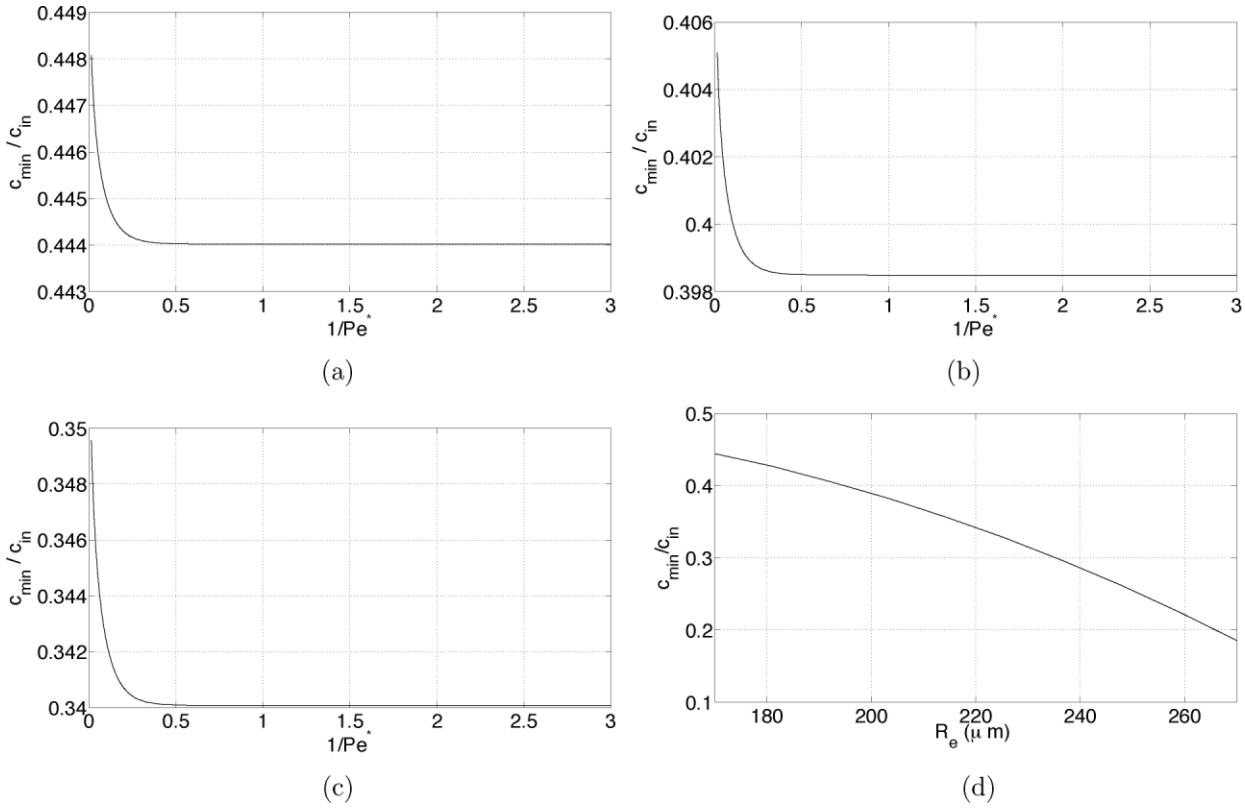


**Figure 3.** Operating equation data for the neonatal rat cardiomyocytes (analytical model). **a**–**c**: The dependence of $c_{min}/c_{in}$ on $1/Pe^*$ when $R_e$ is fixed. **d**: The dependence of $c_{min}/c_{in}$ on $R_e$ when $Pe^*$ is fixed. a: [$R_e = 170\,\mu m$], (b) [$R_e = 195\,\mu m$], (c) [$R_e = 220\,\mu m$], and (d) $Pe^* = 1/3$.

### *Case Study: Cells With a High Oxygen Requirement*

Consider a HFB for culturing cardiomyocytes with the following known parameters: $c_{min} = 8 \times 10^{-2}\,mol\,m^{-3}$, $c_{in} = 0.22\,mol\,m^{-3}$, and $c_{min}/K_m = 11.6$, together with the ECS depth fixed at 95 μm so that $R_e = 215\,\mu m$. For HFB operation it is necessary to specify the inlet flowrate and fiber length to maintain the oxygen concentration above this minimum. Since $c_{min}/K_m > 2$ and the ECS depth is fixed, the analytical approach (operating equation 14) will be used to determine the value of $Pe^*$ (and corresponding possible values of $L$ and $U$) that achieves $c_{min}/c_{in} = 0.36$. For this scenario, $A = 0.80$ and the values of $B_n$ and $C_n$ for $n = 0, \ldots, 49$ are given in the Supplementary Material C. Solving operating equation (14) yields $Pe^* = 0.2$ so that the ratio $U/L = 6 \times 10^{-2}$. Any values of $U$ and $L$ that satisfy this ratio will ensure $c > 8 \times 10^{-2}\,mol\,m^{-3}$ throughout the construct; two example values are $L = 0.1\,m$ and $U = 6 \times 10^{-3}\,m\,s^{-1}$.

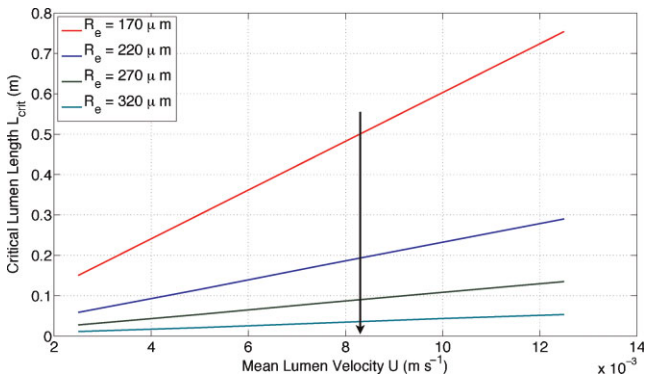


**Figure 4.** Numerical results for the neonatal rat cardiomyocytes that show the relationship between $L_{crit}$ and $U$ when $c_{min} = 6 \times 10^{-3}\,mol\,m^{-3}$ and $c_{min}/K_m = 0.87$ are held fixed (arrow in direction of $R_e$ decreasing). [Color figure can be seen in the online version of this article, available at http://wileyonlinelibrary.com/bit]

By comparison, suppose the lumen flow velocity is fixed at $U = 1 \times 10^{-2}\,m\,s^{-1}$ and the lumen length at $L = 0.1\,m$ so that $Pe^* = 1/3$. Then operating equation (17) can be used to determine the ECS depth that achieves $c_{min}/c_{in} = 0.36$. For this scenario, $K = 1.01$ and $Q = 1.18 \times 10^6\,m^{-2}$, and the values of $H_n$ and $J_n$ for $n = 0, \ldots, 49$ are given in the Supplementary Material C. Solving operating equation (17) with $c_{min}/c_{in} = 0.36$ now gives $R_e = 212.8\,\mu m$ so that the ECS depth is 92.8 μm.

### *Case Study: Cells With a Low Oxygen Requirement*

Next consider a HFB for culturing chondrocytes with the following known parameters: $c_{min} = 2.2 \times 10^{-3}\,mol\,m^{-3}$,

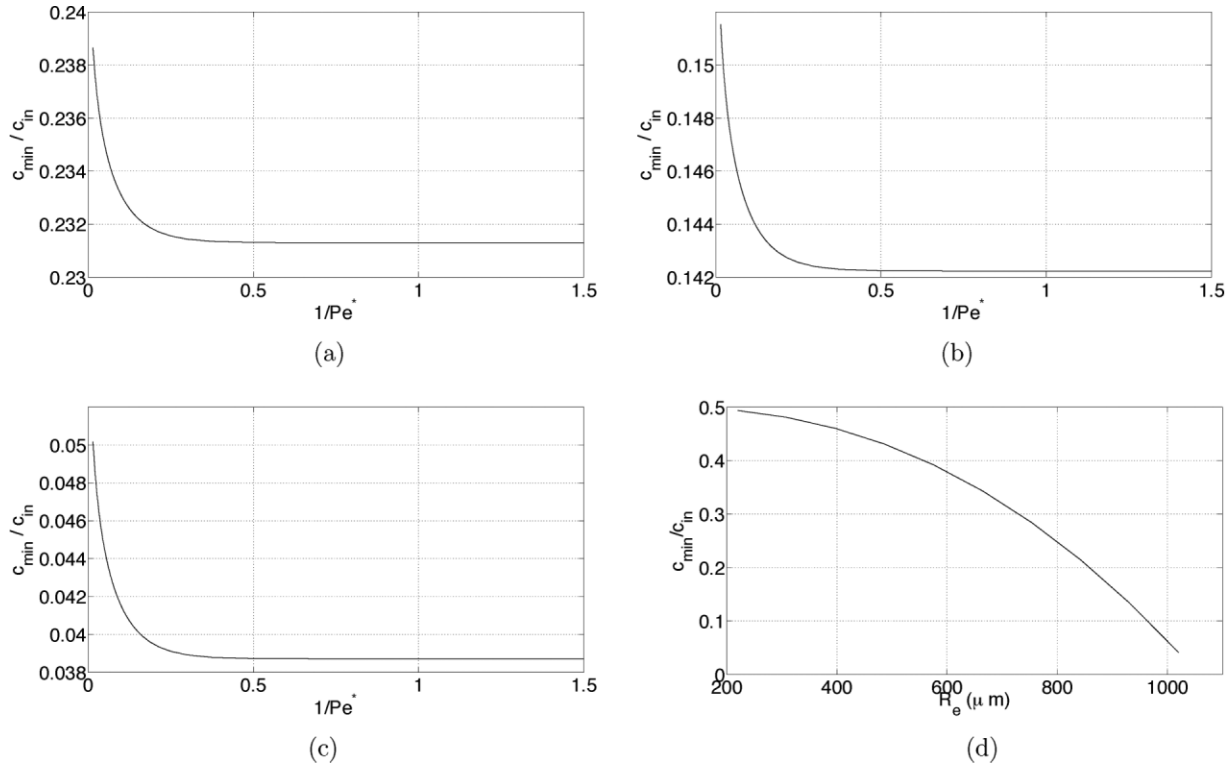


**Figure 5.** Operating equation data for the bovine chondrocytes (analytical model). **a**–**c**: The dependence of $c_{min}/c_{in}$ on $1/Pe^*$ when $R_e$ is fixed. **d**: The dependence of $c_{min}/c_{in}$ on $R_e$ when $Pe^*$ is fixed. a: [$R_e = 820\,\mu m$], (b) [$R_e = 920\,\mu m$], (c) [$R_e = 1{,}020\,\mu m$], and (d) $Pe^* = 1/3$.

$c_{in} = 0.1\,mol\,m^{-3}$, and $c_{min}/K_m = 0.44$, together with the ECS depth fixed at $150\,\mu m$ so that $R_e = 270\,\mu m$. It is necessary to specify the inlet flowrate and fiber length to maintain the oxygen concentration above this minimum. Since $c_{min}/K_m \leq 2$ and the ECS depth is fixed, the numerical approach will be used to determine possible values of $L$ and $U$ that achieve $c_{min}/c_{in} = 2.2 \times 10^{-2}$. For this scenario, we refer to Figure 6. Any values of $L$ and $U$ that lie on the blue line ($R_e = 270\,\mu m$) are appropriate: an example is $U = 2.8 \times 10^{-4}\,m\,s^{-1}$ and $L = 0.2\,m$.By comparison, suppose the lumen flow velocity is fixed at $U = 3 \times 10^{-4}\,m\,s^{-1}$ and lumen length $L = 0.5$. The red line of Figure 6 dictates that $R_e = 170\,\mu m$ should be imposed in this case.

## Discussion

The strategy that has been outlined enables mathematical modeling techniques to inform bioreactor design based on the oxygen requirements of the cell type. Two different modeling approaches were employed to provide design and operating data that ensure the oxygen concentration throughout a HFB is held above a prescribed tissue-specific minimum value, $c_{min}$ that ensures the growth of a functional cell population. When $c_{min} \gg K_m$ (the half-maximal oxygen concentration), oxygen uptake by the cell population was captured using zero-order kinetics, and operating equations were derived analytically. These operating equations provide insight into the relationship between the minimum oxygen concentration and the geometrical properties of the bioreactor, together with the operational parameters (such as inlet oxygen concentration and flow rate) than can be controlled by the user. A case study was presented that demonstrated how to use these operating equations for cell types with a high oxygen requirement. However, an analytical approach is not valid when $c_{min} \not\gg K_m$. In this case, full Michaelis–Menten kinetics must be solved in the ECS using a numerical approach. This was achieved using the finite elements package "COMSOL Multiphysics," and operating data on the relationship between lumen length and flow rate required to achieve a specific minimum oxygen concentration value were presented. This approach has the advantage of being valid for all concentration values; however, the full system of equations must be solved iteratively each time and this is a computationally intensive process. A case study was presented that demonstrated how to use these operating equations for cell types with a low oxygen requirement.

Previous studies into the modeling of tissue engineering bioreactors have focused on either numerical or analytical approaches (under various simplifying assumptions) in isolation. For example, Abdullah and Das (2007), Chen

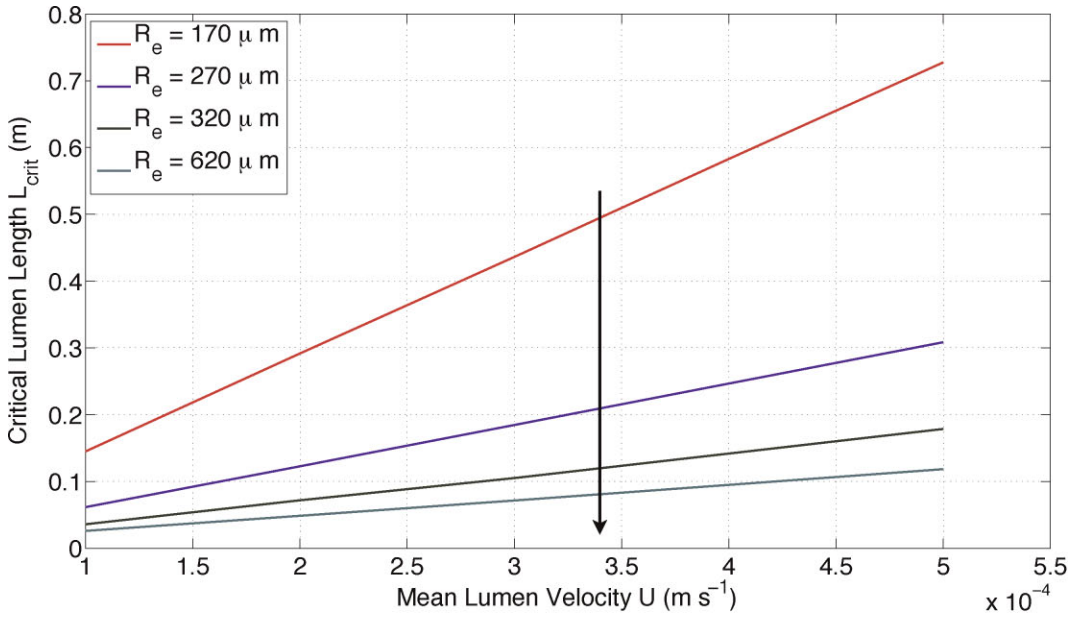


(a)

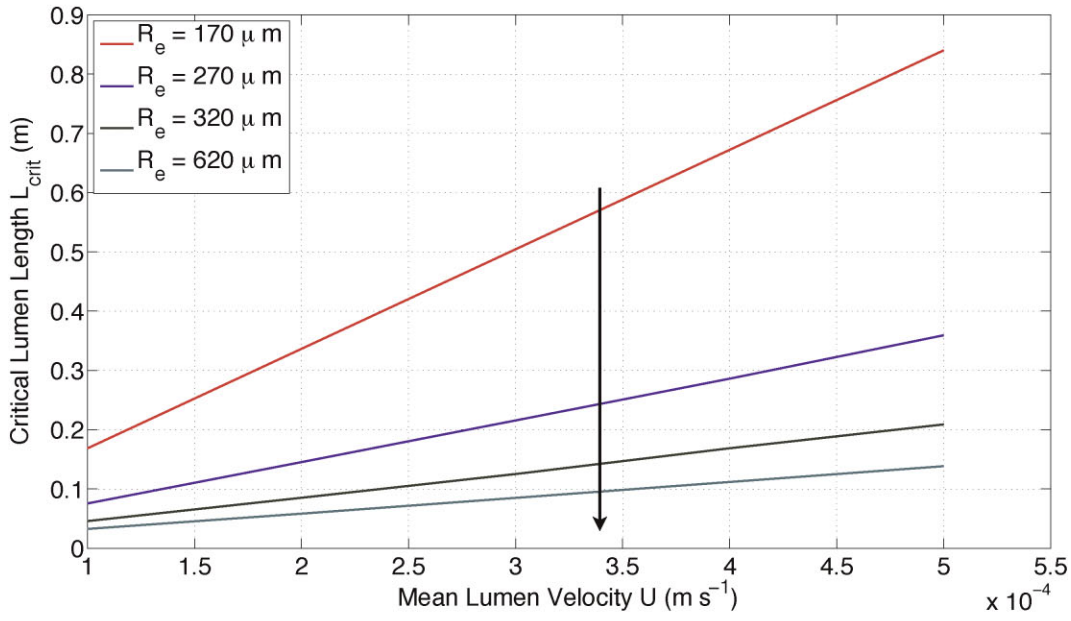


(b)

**Figure 6.** Numerical results for the bovine chondrocytes that show the relationship between $L_{crit}$ and $U$ for two different minimum oxygen requirements (arrows in direction of $R_e$ decreasing). **a**: [$c_{min} = 1 \times 10^{-2}$ mol m$^{-3}$ and $c_{min}/K_m = 2.0$ held fixed], (b) [$c_{min} = 2.2 \times 10^{-3}$ mol m$^{-3}$ and $c_{min}/K_m = 0.44$ held fixed]. [Color figure can be seen in the online version of this article, available at http://wileyonlinelibrary.com/bit]

and Palmer (2010), Das (2007), Pillarella and Zydney (1990), Sullivan et al. (2007, 2008), and Ye et al. (2006) employed various numerical techniques to solve full Michaelis–Menten kinetics for individual cell types in HFBs. By comparison, analytical approaches such as Piret and Cooney (1991), Jayaraman (1992), and Kim and Cooney (1976) have been used to approximate Michaelis–Menten by zero- or first-order kinetics. However, zero-order kinetics have not previously been used to determine operating equations, whilst first-order kinetics are only valid when the substrate concentration is smaller than the half-maximal substrate concentration, $K_m$. This is not appropriate in the development of oxygen-based operating equations for the use of HFB for tissue engineering, where

the oxygen concentration must typically be maintained above $K_m$ to ensure the growth of functional tissue. While these are all valid and workable models, they have not previously been integrated to provide a strategy that could be applied to any cell type to stipulate bioreactor design and operation.

## Conclusion

A strategy has been developed for modeling oxygen kinetics in tissue engineering HFB. The strategy allows operating parameters to be specified that ensure the oxygen concentration is maintained above a prescribed minimum throughout the HFB. The strategy dictates that the appropriate approach is based on whether the Michaelis–Menten kinetics can be reduced to zero-order; in the case of high oxygen requirements zero-order kinetics is appropriate and so the analytical approach is used. In the case of low oxygen requirements it is necessary to use full Michaelis–Menten kinetics and so a numerical approach is required. As such, the strategy developed here can be used for any cell type to specify operating parameters.

## Nomenclature

| | |
|---|---|
| $d$ | radius of the lumen (m) |
| $s$ | depth of the lumen wall (m) |
| $l$ | depth of the ECS (m) |
| $L$ | length of a single module (m) |
| $L_{\text{crit}}$ | critical length required to satisfy a minimum oxygen requirement (m) |
| $z$ | axial length coordinate down the lumen |
| $r$ | radial coordinate |
| $\mathbf{u}$ | fluid velocity vector ($\text{m s}^{-1}$) |
| $U$ | Mean velocity in the lumen ($\text{m s}^{-1}$) |
| $\mathbf{e}_z$ | unit vector in the $z$-direction |
| $c$ | oxygen concentration ($\text{mol m}^{-3}$) |
| $\mathbf{J}$ | oxygen flux ($\text{mol m}^{-2}\,\text{s}^{-1}$) |
| $U$ | velocity scale ($\text{m s}^{-1}$) |
| $D_l$ | oxygen diffusion coefficient in the lumen ($\text{m}^2\,\text{s}^{-1}$) |
| $D_w$ | oxygen diffusion coefficient in the wall ($\text{m}^2\,\text{s}^{-1}$) |
| $D_e$ | oxygen diffusion coefficient in the ECS ($\text{m}^2\,\text{s}^{-1}$) |
| $R$ | uptake rate of oxygen ($\text{mol m}^{-3}\,\text{s}^{-1}$) |
| $V_{\max}$ | Maximal oxygen consumption rate ($\text{mol m}^{-3}\,\text{s}^{-1}$) |
| $K_m$ | half-maximal oxygen concentration ($\text{mol m}^{-3}$) |
| $\mathbf{n}$ | unit outward pointing normal to a surface |
| $c_{\text{in}}$ | fixed oxygen concentration at the lumen inlet ($\text{mol m}^{-3}$) |
| $c_{\min}$ | minimum oxygen concentration in the HFB ($\text{mol m}^{-3}$) |
| $\varepsilon$ | aspect ratio of the lumen |
| $Pe$ | axial Péclet number in the lumen |
| $Pe^*$ | reduced Péclet number in the lumen |
| $R_l$ | outer lumen radius (m) |
| $R_m$ | outer membrane radius (m) |
| $R_e$ | outer ECS radius (m) |
| $M$ | dimensionless constant that represents the balance of oxygen consumption versus diffusion in the ECS |
| $\gamma$ | algebraically convenient parameter that depends on $R_e$ |
| $\lambda_n$ | eigenvalues of Sturm–Liouville problem for $n = 0, \ldots, \infty$ |
| $E_n$ | normalization constants of Sturm–Liouville problem for $n = 0, \ldots, \infty$ |
| $F_n$, $G_n$ | Sturm–Liouville expansion constants for $n = 0, \ldots, \infty$ |
| $B(z)$ | dimensionless oxygen concentration on the lumen wall |
| $A$, $B_n$, $C_n$, $K$, $Q$, $H_n$, $J_n$ | constants associated with the analytic operating equations |

This work was funded by Christ Church and the Mathematical Institute, University of Oxford, together with the Department of Chemical Engineering, University of Bath. S.L.W. is grateful to the EPSRC for funding in the form of an Advanced Research Fellowship. R.J.S. is grateful to the University of Oxford for funding in the form of a John Fell Fund Oxford University Press Grant.

## References

Abdullah N, Das D. 2007. Modelling nutrient transport in hollow fibre membrane bioreactor for growing bone tissue with consideration of multi-component interactions. Chem Eng Sci 62:5821–5839.

Abdullah N, Jones D, Das D. 2009. Nutrient transport in bioreactors for bone tissue growth: Why do hollow fibre membrane bioreactors work? Chem Eng Sci 64(1):109–125.

Abramowitz M, Stegun IA. 1964. Handbook of mathematical functions with formulas, graphs, and mathematical tables. Dover Publications.

Brotherton J, Chau P. 1996. Modeling of axial-flow hollow fiber cell culture bioreactors. Biotechnol Prog 12(5):575–590.

Carrier R, Papadaki M, Rupnick M, Schoen F, Bursac N, Langer R, Freed L, Vunjak-Novakovic G. 1999. Cardiac tissue engineering: Cell seeding, cultivation parameters, and tissue construct characterization. Biotechnol Bioeng 64(5):580–589.

Chen G, Palmer A. 2010. Mixtures of hemoglobin-based oxygen carriers and peruorocarbons exhibit a synergistic effect in oxygenating hepatic hollow fiber bioreactors. Biotechnol Bioeng 105(3):534–542.

Consolo F, Fiore G, Truscello S, Caronna M, Morbiducci U, Montevecchi F, Redaelli A. 2008. A compu-tational model for the optimization of transport phenomena in a rotating hollow-fiber bioreactor for artificial liver. Tissue Eng Part C Methods 15(1):41.

Das D. 2007. Multiscale simulation of nutrient transport in hollow fibre membrane bioreactor for growing bone tissue: Sub-cellular scale and beyond. Chem Eng Sci 62(13):3627–3639.

Ellis M, Chaudhuri J. 2007. Poly (lactic-co-glycolic acid) hollow fibre membranes for use as a tissue engineering scaffold. Biotechnol Bioeng 96(1):177–187.

Ellis M, Jarman-Smith M, Chaudhuri JB. 2005. Bioreactors for tissue engineering. Amsterdam: Kluwer Academic Publishers.

Fermor B, Christensen S, Youn I, Cernanec J, Davies C, Weinberg J. 2007. Oxygen, nitric oxide and articular cartilage. Eur Cell Mater 13:56–65.

Gloeckner H, Lemke H. 2001. New miniaturized hollow-fiber bioreactor for in vivo like cell culture, cell expansion, and production of cell-derived products. Biotechnol Prog 17:828–831.

Gramer M, Poeschl DM. 2000. Comparison of cell growth in T-Flasks, in micro hollow fiber biroeactors, and in an industrial scale hollow fiber bioreactor. Cytotechnology 34:111–119.

Hay P, Veitch A, Smith M, Cousins R, Gaylor J. 2000. Oxygen transfer in a diffusion-limited hollow fiber bioartificial liver. Artif Organs 24(4): 278–288.

Jayaraman V. 1992. The solution of hollow-fiber bioreactor design equations. Biotechnol Prog 8(5):462–464.

Kawazoe Y, Eguchi S, Sugiyama N, Kamohara Y, Fujioka H, Kanematsu T. 2006. Comparison between bioartificial and artificial liver for the treatment of acute liver failure in pigs. World J Gastroenterol 12(46):7503.

Kim S, Cooney D. 1976. An improved theoretical model for hollow-fiber enzyme reactors. Chem Eng Sci 31(4):289–294.

Knazek R, Gullino P, Kohler P, Dedrick R. 1972. Cell culture on artificial capillaries: An approach to tissue growth in vitro. Science 178:65–67.

Krogh A. 1918. The rate of diffusion of gases through animal tissue with some remarks on the coefficient of invasion. J Physiol 52:391.

Lund-Olesen K. 1970. Oxygen tension in synovial fluids. Arthritis Rheum 13(6):769–776.

Malda J, Rouwkema J, Martens D, le Comte E, Kooy F, Tramper J, van Blitterswijk C, Riesle J. 2004. Oxygen gradients in tissue-engineered PEGT/PBT cartilaginous constructs: Measurement and modeling. Biotechnol Bioeng 86(1):9–18.

Martin Y, Vermette P. 2005. Bioreactors for tissue mass culture: Design, characterization, and recent advances. Biomaterials 26(35):7481–7503.

Nyberg S, Remmel RP, Mann HJ, Peshwa MV, Hu WS, Cerra FB. 1994. Primary hepatocytes outperform Hep G2 cells as the source of biotransformation functions in a bioartificial liver. Ann Surg 220:59–67.

Nyberg S, Hardin J, Amiot B, Argikar U, Remmel R, Rinaldo P. 2005. Rapid, large-scale formation of porcine hepatocyte spheroids in a novel spheroid reservoir bioartificial liver. Liver Transplant 11(8):901–910.

Obradovic B, Carrier R, Vunjak-Novakovic G, Freed L. 1999. Gas exchange is essential for bioreactor cultivation of tissue engineered cartilage. Biotechnol Bioeng 63(2):197–205.

Obradovic B, Meldon J, Freed L, Vunjak-Novakovic G. 2000. Glycosaminoglycan deposition in engineered cartilage: Experiments and mathematical model. AIChE J 46(9):1860–1871.

Patzer J II. 2004. Oxygen consumption in a hollow fiber bioartificial liver revisited. Artif Organs 28(1):83–98.

Pillarella M, Zydney A. 1990. Theoretical analysis of the effect of convective ow on solute transport and insulin release in a hollow fiber bioartificial pancreas. J Biomech Eng 112:220.

Piret J, Cooney C. 1991. Model of oxygen transport limitations in hollow fiber bioreactors. Biotechnol Bioeng 37(1):80–892.

Radisic M, Deen W, Langer R, Vunjak-Novakovic G. 2005. Mathematical model of oxygen distribution in engineered cardiac tissue with parallel channel array perfused with culture medium containing oxygen carriers. Am J Physiol Heart Circ Physiol 288(3):H1278–H1289.

Scragg A. 1991. Bioreactors in biotechnology: A practical approach. Chichester, West Sussex: Ellis Horwood Limited.

Shipley R, Waters S, Ellis M. 2010. Definition and validation of operating equations for poly(vinyl alcohol)-poly(lactide-co-glycolide) microfiltration membrane-scaffold bioreactors. Biotechnol Bioeng. 107(2): 382–392.

Sielaff T, Nyberg S, Rollins M, Hu M, Amiot B, Lee A, Wu F, Hu W, Cerra F. 1997. Characterization of the three-compartment gel-entrapment porcine hepatocyte bioartificial liver. Cell Biol Toxicol 13(4):357–364.

Stabler C, Fraker C, Pedraza E, Constantinidis I, Sambanis A. 2009. Modeling and in vitro and in vivo characterization of a tissue engineered pancreatic substitute. J Comb Optim 17(1):54–73.

Sullivan JP, Gordon JE, Bou-Akl T, Matthew HWT, Palmer AF. 2007. Enhanced oxygen delivery to primary hepatocytes within a hollow fiber bioreactor facilitated via hemoglobin-based oxygen carriers. Artif Cells Blood Substit Immobil Biotechnol 35(6):585–606.

Sullivan J, Harris D, Palmer A. 2008. Convection and hemoglobin-based oxygen carrier enhanced oxygen transport in a hepatic hollow fiber bioreactor. Artif Cells Blood Substit Biotechnol 36(4):386–402.

Tharakan J, Chau P. 1986. Operation and pressure distribution of immobilized cell hollow fiber bioreactors. Biotech Bioeng 28:1064–1071.

Treuhaft P, McCarty D. 1971. Synovial fluid pH, lactate, oxygen and carbon dioxide partial pressure in various joint diseases. Arthritis Rheum 14(4):475–484.

Tziampazis E, Sambanis A. 1995. Tissue engineering of a bioartificial pancreas - modeling the cell environment and device function. Biotechnol Prog 11(2):115–126.

Wurm M, Woess C, Libiseller K, Beer B, Pavlic M. 2009. Challenging small human hepatocytes with opiates: Further characterization of a novel prototype bioartificial liver. Tissue Eng Part A 16(3):807–813.

Ye H, Das D, Trifftt J, Cui Z. 2006. Modelling nutrient transport in hollow fibre membrane bioreactors for growing three-dimensional bone tissue. J Membr Sci 272(1–2):169–178.

Ye H, Xia Z, Ferguson D, Trifftt J, Cui Z. 2007. Studies on the use of hollow fibre membrane bioreactors for tissue generation by using rat bone marrow fibroblastic cells and a composite scaffold. J Mater Sci Mater Med 18(4):641–648.